Independent normalization for γ-ray strength functions: The shape method

M. Wiedeking,[1,2,*] M. Guttormsen,[3] A. C. Larsen,[3] F. Zeiser,[3] A. Görgen,[3] S. N. Liddick,[4,5] D. Mücher,[6,7] S. Siem,[3] and A. Spyrou[4,8]

[1]*Department of Subatomic Physics, iThemba LABS, P.O. Box 722, Somerset West 7129, South Africa*
[2]*School of Physics, University of the Witwatersrand, Johannesburg 2050, South Africa*
[3]*Department of Physics, University of Oslo, NO-0316 Oslo, Norway*
[4]*National Superconducting Cyclotron Laboratory, Michigan State University, East Lansing, Michigan 48824, USA*
[5]*Department of Chemistry, Michigan State University, East Lansing, Michigan 48824, USA*
[6]*Department of Physics, University of Guelph, Guelph, Ontario, Canada N1G 2W1*
[7]*TRIUMF, 4004 Wesbrook Mall, Vancouver, British Columbia, Canada V6T 2A3*
[8]*Department of Physics and Astronomy and Joint Institute for Nuclear Astrophysics, Michigan State University, East Lansing, Michigan 48824, USA*

(Received 24 October 2020; revised 16 February 2021; accepted 14 June 2021; published 12 July 2021)

The shape method, a novel approach to obtain the functional form of the γ-ray strength function (γSF), is introduced. In connection with the Oslo method the slope of the nuclear level density (NLD) and γSF can be obtained simultaneously even in the absence of neutron resonance spacing data. The foundation of the shape method lies in the primary γ-ray transitions which preserve information on the functional form of the γSF. The shape method has been applied to ^{56}Fe, ^{92}Zr, and ^{164}Dy, which are representative cases for the variety of situations encountered in typical NLD and γSF studies. The comparisons of results from the shape method to those from the Oslo method demonstrate that the functional form of the γSF is retained regardless of nuclear structure details or J^{π} values of the states fed by the primary transitions.

DOI: 10.1103/PhysRevC.104.014311

I. INTRODUCTION

The number of nuclear levels per energy interval, the nuclear level density (NLD), and the γ-ray strength function (γSF), which is a measure of the average reduced γ-ray decay probability, have received significant experimental and theoretical attention over the last decade. The necessity for reliable γSF data has compelled the International Atomic Energy Agency to establish a dedicated γSF database together with recommendations [1]. The demand for γSFs and NLDs is driven in part due to their relevance to astrophysical nucleosynthesis via capture processes [2–5]. Recent experimental results have clearly demonstrated that capture cross sections can be reliably obtained using NLDs and γSFs as input into reaction models [6–9], which are based on the Hauser-Feshbach approach [10].

Several experimental methods exist [1] to extract γSFs from experimental data, and of those the Oslo method [11] has been extensively used. The advantage of the Oslo method lies in its ability to simultaneously extract the γSF and NLD from particle-γ coincident data albeit with the need of external normalization. The NLD and γSF are traditionally normalized by three external parameters: (i) the NLD is normalized to the level densities of discrete states at low excitation energies, (ii) the NLD at the neutron separation energy (S_n) is constrained to the s-wave neutron resonance spacing (D_0), and (iii) the absolute value of the γSF is determined from the average total radiative width of s-wave resonances ($\langle\Gamma_{\gamma 0}\rangle$). The functional form of the NLD is linked to that of the γSF and can be fully constrained by normalizations (i) and (ii) above. The γSFs extracted with the Oslo method have been shown to be reproduced using alternative methods, which do not rely on external models or normalization [12–14].

Difficulties in normalizing NLD and γSF data from the Oslo method emerge for nuclei without available D_0 and/or $\langle\Gamma_{\gamma 0}\rangle$ values. This is the case for many nuclei A when $A-1$ targets are difficult or even impossible to manufacture, due to the physical or chemical properties of the isotopes and elements, respectively. The lack of D_0 and $\langle\Gamma_{\gamma 0}\rangle$ data present challenges for the normalization of NLDs and γSFs. In the absence of normalization data, no coherent prescription is currently available as case-specific approaches [7,8,15–17] do not appear to be consistently applicable. Even in cases where D_0 is known, the normalization procedure introduces a model dependence, which can lead to large uncertainties [1,18]. A reliable approach is highly desirable, especially since the required data needs driven by nucleosynthesis studies primarily involve nuclei for which direct measurements of capture cross sections as well as D_0 and $\langle\Gamma_{\gamma 0}\rangle$ values are not possible. Experimentally, γSF and NLD data for nuclei away from the line of stability are readily reachable however, in particular with recent advances in extending the Oslo method to previously inaccessible regions through the β-Oslo [7,15,19] and inverse-Oslo [20] methods.

*wiedeking@tlabs.ac.za

In this paper, the *shape method* is introduced, which is a novel and mostly model independent approach to determine the slope of NLDs and γSFs extracted with the Oslo method in the absence of measured D_0 values. We have also applied the shape method to β-decay data on ^{76}Ge and ^{88}Kr to explore the extraction of model-independent NLDs away from stability [21]. In Sec. II the Oslo method and the normalization for NLDs and γSFs are reviewed. Section III presents the concepts and details of the shape method, which allows for the normalization of NLDs and γSFs. Section IV focuses on the shape method analysis and results on ^{56}Fe, ^{92}Zr, and ^{164}Dy. The discussion of results together with recommendations on the use and applicability of the shape method is provided in Sec. V. Summarizing remarks are made in Sec. VI.

II. REVIEW OF THE OSLO METHOD AND NORMALIZATIONS

The Oslo method [11] extracts the γSF and NLD simultaneously through the following procedure: States in the quasi-continuum (below the particle threshold) are typically populated with charged-particle direct and scattering reactions or following β decay. The γ-ray spectrum is unfolded with the detector response function using an iterative subtraction technique [22]. From the unfolded spectra, and with the assumption that the residual nucleus reaches a compound state, the primary γ-ray spectrum is obtained through the first-generation method [23]. The first-generation matrix $P(E_i, E_\gamma)$ is proportional to the γ-ray decay probability and can be factorized according to the expression that is derived from the compound nucleus formalism (details are found in Appendix C of Ref. [24])

$$P(E_\gamma, E_i) \propto \rho(E_f)\mathcal{T}(E_\gamma), \tag{1}$$

where $\rho(E_f)$ is the nuclear level density and $\mathcal{T}(E_\gamma)$ is the transmission coefficient, which is independent of excitation energy (E_i) and hence nuclear temperature. This follows from the generalized Brink-Axel hypothesis [25], which states that collective excitation modes built on excited states have the same properties as those built on the ground state. The hypothesis has been validated in the quasicontinuum with the Oslo method in ^{238}Np [26], ^{116,120,124}Sn [27], ^{64,65}Ni [28], and ^{56,57}Fe [29]. The theoretical matrix $P_{th}(E_\gamma, E_i)$ is given by [11]

$$P_{th}(E_\gamma, E_i) = \frac{\rho(E_f)\mathcal{T}(E_\gamma)}{\sum_{E_\gamma}\rho(E_f)\mathcal{T}(E_\gamma)}. \tag{2}$$

The $\rho(E_f)$ and $\mathcal{T}(E_\gamma)$ can be simultaneously extracted by performing a χ^2 minimization between the theoretical $P_{th}(E_\gamma, E_i)$ and experimental $P(E_\gamma, E_i)$ first-generation matrices [11].

From Eq. (2) an infinite number of solutions are obtained, and the physical solution is found by normalizing $\mathcal{T}(E_\gamma)$ and $\rho(E_f)$ to experimental data [11] with

$$\tilde{\rho}(E_f) = A\rho(E_f)e^{\alpha E_f} \tag{3}$$

and

$$\tilde{\mathcal{T}}(E_\gamma) = B\mathcal{T}(E_\gamma)e^{\alpha E_\gamma}, \tag{4}$$

where A and B are constants and α is the transformation that affects the common slope. The slope α and constant A are determined by the NLD of the known discrete states at lower excitation energies and the total NLD at S_n. The functional form of $\rho(E_f)$ and $\mathcal{T}(E_\gamma)$ is defined from the χ^2 fit to the primary γ-ray matrix $P(E_\gamma, E_i)$. For a detailed discussion and implementation of the Oslo method, see Ref. [24].

In this work, data from ^{56}Fe [30], ^{92}Zr [31], and ^{164}Dy [32] have been reanalyzed with the Oslo method using an intrinsic spin-distribution for the absolute normalization at S_n. The γSFs of those nuclei may therefore deviate slightly from results presented in previous publications. The form of the spin-distribution is assumed to follow [33]

$$g(E, J) \simeq \frac{2J+1}{2\sigma^2(E)}\exp[-(J+1/2)^2/2\sigma^2(E)], \tag{5}$$

where E is the excitation energy, J the spin, and the spin cutoff parameter $\sigma(E)$ is assumed to have the functional form [34,35]

$$\sigma^2(E) = \sigma_d^2 + \frac{E-E_d}{S_n-E_d}\left[\sigma^2(S_n) - \sigma_d^2\right], \tag{6}$$

determined by two excitation energies. At the lower excitation energy $E = E_d$, we determine the spin cutoff parameter σ_d from known discrete levels. The second point at $E = S_n$ is estimated assuming a rigid moment of inertia [36,37]

$$\sigma^2(S_n) = 0.0146A^{5/3}\frac{1+\sqrt{1+4aU_n}}{2a}, \tag{7}$$

where A is the mass number, a is the NLD parameter, $U_n = S_n - E_1$ is the intrinsic excitation energy, and E_1 is the energy-shift parameter.

At S_n, normalization is achieved from NLDs calculated with [11]

$$\rho(S_n) = \frac{2\sigma^2(S_n)}{D_0\left((J_t+1)\exp\left[-\frac{(J_t+1)^2}{2\sigma^2(S_n)}\right] + J_t\exp\left[-\frac{J_t^2}{2\sigma^2(S_n)}\right]\right)}. \tag{8}$$

The experimental D_0 value is obtained from $\ell = 0$ (s-wave) neutron resonance spacing data which are typically retrieved from Refs. [35,38] and J_t is the initial spin of the target nucleus. Generally, NLDs can only be extracted to excitation energies well below S_n with the Oslo method. The absolute normalization at S_n, which sensitively depends on the spin distribution, is achieved by extrapolating the NLDs using a variety of level density models, such as the back-shifted Fermi-gas [39], the constant temperature [40], or the Hartree-Fock-Bogoliubov-plus-combinatorial [41] models.

The absolute normalization parameter B in Eq. (4) is obtained by constraining the experimental data to $\langle\Gamma_{\gamma 0}\rangle$ for s-wave resonances by [24,42]

$$\langle\Gamma_{\gamma 0}(S_n)\rangle = \frac{1}{2\pi\,\rho(S_n, J_t \pm 1/2, \pi_t)} \times \sum_{J_f}\int_0^{S_n} B\mathcal{T}(E_\gamma)\rho(S_n - E_\gamma, J_f)dE_\gamma, \tag{9}$$

TABLE I. Parameters used for the extraction of NLDs and γSFs (see text for details).

Nucleus	S_n (MeV)	D_0 (eV)	a[c] (MeV^{-1})	E_1[c] (MeV)	E_d (MeV)	σ_d	$\sigma(S_n)$	$\rho(S_n)$ (MeV^{-1})	T_{CT} (MeV)	$\langle\Gamma_\gamma\rangle$ (meV)
^{56}Fe	11.197		6.196	0.94	2.70	2.5	4.05	2870(680)[d]	1.35(5)	1900(600)[d]
^{92}Zr	8.635	514(15)[a]	10.4	0.66	3.0	3.0	4.50	16640(490)	0.90(2)	131(56)
^{164}Dy	7.658	6.8(6)[b]	18.12	0.31	1.09	3.6	6.91	$2.59(52)\times10^6$	0.59(2)	113(13)

[a]Value from [38].
[b]Value from [35].
[c]Values from [36,37].
[d]Estimated from systematics corresponding to *norm-2* in Ref. [29].

where π_t is the parity of the target nucleus in the (n,γ) reaction, J_f and J_t are the spins of the levels in the final and target nucleus, respectively.

The essential parameters used here for the extraction of the NLDs and γSFs are listed in Table I. More details on the extraction of NLDs and γSFs for ^{56}Fe, ^{92}Zr, and ^{164}Dy are discussed in Refs. [30–32].

The relationship between $\mathcal{T}(E_\gamma)$ and the γSF $[f_{XL}(E_\gamma)]$ with XL being the type and multipolarity of the radiation, respectively, is [35]

$$\mathcal{T}_{XL}(E_\gamma) = 2\pi E_\gamma{}^{2L+1} f_{XL}(E_\gamma). \tag{10}$$

With the assumption that statistical γ-ray decay is dominated by dipole transitions, the total γSF $[f(E_\gamma)]$ becomes

$$f(E_\gamma) = f_{E1}(E_\gamma) + f_{M1}(E_\gamma) = \frac{\mathcal{T}(E_\gamma)}{2\pi E_\gamma^3}. \tag{11}$$

The values of D_0 and $\langle\Gamma_{\gamma 0}\rangle$ from s-wave resonance and to a limited extent D_1 and $\langle\Gamma_{\gamma 1}\rangle$ values from p-wave resonance measurements[1] are generally available for nuclei which are populated through (n,γ) reactions on stable targets. For the majority of nuclei the information required by the Oslo method to determine A, B, and α has not been measured, mostly due to the unavailability of targets. This led to many nonstandardized approaches to estimate the values D_0 and $\langle\Gamma_{\gamma 0}\rangle$ [7,8,15–17].

The development of a method with no or only very limited model dependencies, which can be systematically applied to nuclei, is of utmost importance to obtain the normalization when D_0 and $\langle\Gamma_{\gamma 0}\rangle$ values are not available. A new method, the shape method, will now be described, which provides a prescription for the normalization of the slope of the NLD and γSF in the absence of D_0. Software for the Oslo and shape (`diablo.c`) methods are available from Refs. [24,43].

III. THE SHAPE METHOD

In this section, the shape method is presented. The method utilizes concepts from γSF measurements using the average resonance capture approach and from the ratio and χ^2 methods using particle-γ-γ coincident data. These approaches are briefly summarized before we continue with a detailed description of the shape method.

A. Average resonance capture

The methodology for average resonance capture [44–46] is similar for beams of protons or neutrons, and several resonances are populated and combined in specific excitation-energy ranges. The shape method will be applied following charged particle reactions and we will focus on the example of average resonance capture with proton beams. Experimental data from (p,γ) reactions have been used to deduce the γSFs for several $45 < A < 91$ nuclei for which the proton separation energy (S_p) is located below S_n, see for example Refs. [1,47,48]. The use of high-resolution detectors allows for the identification of individual primary γ-ray transitions to low-lying levels as long as the resolution of the proton beam is better than the spacing of low-lying levels. The relative intensities of primary transitions (corrected by E_γ^3), which originate from a given excitation energy region and decay to low-lying levels with the same spin and parity, preserve the shape and hence the energy dependence of the γSF. The proton beam energies, together with the target thicknesses, provide an unambiguous assignment of specific excitation energies. Data of primary transitions to low-lying states of different spins and parities (J^π) are normalized by weighting the different contributions through the Hauser-Feshbach formalism. Regardless this normalization, the energy dependence of the γSF remains completely independent of any model input.

B. Ratio and χ^2 Methods

The Ratio method [12] is a model-independent approach to obtain the γ-energy dependence of the γSF from correlated particle-γ-γ events. The γ-γ coincidence is between the primary γ-ray transition, originating from the region of the quasi-continuum populated in the reaction, and the transition from low-lying discrete states, which are fed by the primary γ rays. When a discrete transition from a low-lying state is detected in coincidence with a charged particle, additional stringent requirements are applied to the primary γ ray, so that the energy sum of the discrete and primary transitions is equal to the excitation energy within the energy resolutions of the detectors and particle beams. Any particle-γ-γ event satisfying these conditions provides an unambiguous determination of the origin and destination of the observed primary

[1]A similar treatment as for D_0 can be applied to p-wave neutron resonance spacing data (D_1) and if available may be used to provide additional constraints.

transition. As long as the primary γ rays feed discrete states of the same J^π the shape of the γSF remains independent of model input by analogy with the average resonance proton capture method. The ratio R of intensities N for two different primary γ-ray energies from the same initial excitation energy E_i to discrete low-lying levels of same J^π at energies E_{l_1} and E_{l_2} is

$$R = \frac{f(E_i - E_{l_1})}{f(E_i - E_{l_2})} = \frac{N_{l_1}(E_i)(E_i - E_{l_2})^3}{N_{l_2}(E_i)(E_i - E_{l_1})^3}. \quad (12)$$

When the ratios from different excitation energies are compared, information on the energy dependence of the γSF is obtained as demonstrated from $(d, p\gamma\gamma)$ [12], (p,p'$\gamma\gamma$) [14], $(\vec{\gamma}, \gamma\gamma)$ [49], and $(p, \gamma\gamma)$ [50] reactions.

Data of primary γ-ray intensities from an excitation energy range to different discrete levels of the same J^π and corrected for E_γ^3, can also be fitted with a χ^2 minimization procedure [12,13], referred here as the χ^2 method. The set of data from different initial excitation energies are independent of each other and following the χ^2 minimization, which combines the sets from different excitation energy bins, yields information on the shape of the γSF.

C. Shape Method Procedure

In the above-described methods discrete γ-ray lines were studied with high-resolution germanium detectors. When the total γSF extending across larger excitation and γ-ray energy ranges is to be measured, the Oslo method with high-efficiency detectors, albeit with worse energy resolution, is regularly used. In the following, we will extend the previous techniques and replace the identification of γ-ray lines from discrete levels l_j with diagonals D_j in a particle-γ matrix.

The diagonals D_j are directly related to the first-generation (or primary) $P(E_\gamma, E_i)$ matrix provided by the Oslo method.[2] Figure 1 illustrates the concepts of diagonals and symbols used where one may define a final excitation energy E_f fed from an initial excitation energy E_i by a γ transition with energy E_γ. This is given by $E_i(E_\gamma) = E_\gamma + E_f$ with E_f fixed and the diagonals D_j with different E_f are parallel to each other as schematically shown in Fig. 1. Here, the direct γ-ray decay from E_i to the ground state is simply given by $E_i(E_\gamma) = E_\gamma$ (within the resolutions of the detectors). The diagonals may appear in three variants containing (i) one final state with given J^π, (ii) two or more specific final states, or, in the case of high level density, (iii) a large number of final states (typically >10) with a corresponding average E_f and possibly many different J^π.

The intensities (counts) given by the content of the pixel (E_γ, E_i) for two diagonals are exploited to obtain a pair of data points which are proportional to the γSF.

In the following, we assume a symmetric parity distribution with the spin distribution $g(E_i, J_i)$ of Eq. (5). Furthermore, we assume the population of a typical state at excitation E_i and

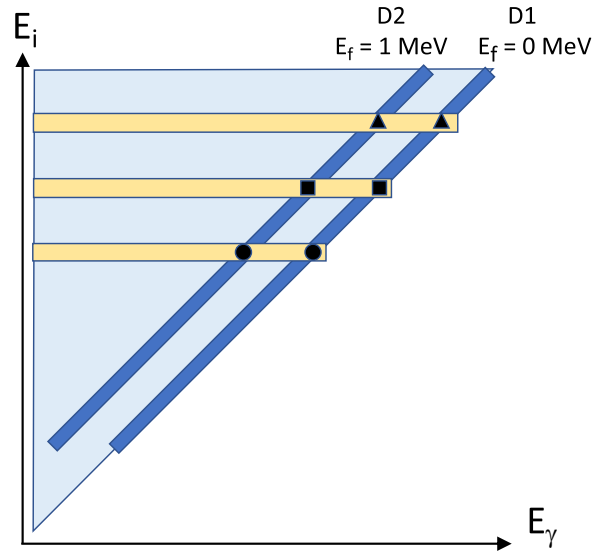

FIG. 1. Illustration of diagonals (blue) D_1 and D_2 selecting specific final states in the $P(E_\gamma, E_i)$ matrix. Horizontal bars (yellow) indicate three initial excitation energies E_i. The number of counts at the crossing points between a diagonal and a bar (E_γ, E_i) gives the intensity of the γ transitions from E_i to $E_i - E_\gamma$, here symbolized with filled circles, squares, and triangles. With intensities from two diagonals at the same E_i, a pair of internally normalized γSF data points can be established.

spin J_i is given by the cross section $\sigma(E_i, J_i)$. The number of counts in a diagonal D_j at (E_γ, E_i) with one or more final J^π states included can then be expressed as a sum of products,

$$N_D \propto \sum_{[J_f]} \sum_{J_i=J_f-1}^{J_i=J_f+1} \sigma(E_i, J_i) g(E_i, J_i) G(E_i, E_\gamma, J_i, J_f), \quad (13)$$

where we define $[J_f]$ as the spins of the final levels within the diagonal; e.g., if the diagonal contains four states with $[J_f]$ then $\sum_{[J_f]}$ is the sum over those four terms. The second sum is restricted to the available J^π populated by dipole transitions connecting initial and final states, which generally includes three initial spins. However, in the case of $J_f = 0$ only the $J_i = 1$ spin is included and for $J_f = 1/2$ only the $J_i = 1/2$ and $J_i = 3/2$ spins are included.

The third factor G in Eq. (13) is proportional to the γ-decay width given by

$$G(E_i, E_\gamma, J_i, J_f) \propto \int_{E_\gamma - \Delta/2}^{E_\gamma + \Delta/2} \mathcal{T}(E_i, E'_\gamma, J_i, J_f) \delta(E_i - E'_\gamma, J_f) dE'_\gamma, \quad (14)$$

where Δ is the energy width of the diagonal which includes the specific final level J_f at $E_f = E_i - E_\gamma$. The δ function assures that one specific level is counted giving $\int \delta \, dE'_\gamma = 1$. With the assumption that the transmission coefficient is almost constant within the energy interval $[E_\gamma - 1/2\Delta, E_\gamma + 1/2\Delta]$, it can be placed outside the integral with a value of $\mathcal{T}(E_i, E_\gamma, J_i, J_f)$.

According to the generalized Brink-Axel hypothesis, the transmission coefficient $\mathcal{T}(E_i, E_\gamma, J_i, J_f)$ is assumed to be

[2]The total γ-ray matrix (all γ rays in a cascade) may be utilized, as long as it is certain that the diagonals contain only primary transitions.

independent of spin, parity, and excitation energy. Thus, we replace the expression for the transmission coefficient by $\mathcal{T}(E_\gamma)$, i.e., a function only dependent of E_γ. Furthermore, if we assume the dominance of dipole transitions in the quasi-continuum region, the transmission coefficient can be replaced by the γSF through $\mathcal{T}(E_\gamma) = 2\pi f(E_\gamma)E_\gamma^3$ from Eq. (11).

With the considerations above, Eq. (13) can be written as

$$N_D \propto f(E_\gamma)E_\gamma^3 \sum_{[J_f]} \sum_{J_i=J_f-1}^{J_i=J_f+1} \sigma(E_i, J_i)g(E_i, J_i). \quad (15)$$

In the following we will assume that the probability of populating a certain initial state with spin J_i at a given E_i is approximately independent of spin, i.e., $\sigma(E_i, J_i) \approx \sigma(E_i, J_i')$.

The shape method applies for the same E_i but for two different diagonals D_1 and D_2; see Fig. 1. We choose diagonal D_1 to represent a lower final excitation energy E_{f1} and D_2 a higher final excitation energy E_{f2}. At the initial excitation energy E_i, the γ-ray energies are $E_{\gamma_1} = E_i - E_{f1}$ and $E_{\gamma_2} = E_i - E_{f2}$ for diagonals D_1 and D_2, respectively.

The strength functions at E_{γ_1} and E_{γ_2} are determined by the number of counts at the diagonals D_1 and D_2 for the same initial excitation energy E_i, using Eq. (15):

$$f(E_{\gamma 1}) \propto \frac{N_{D1}}{E_{\gamma 1}^3 \sum_{[J_{f1}]} \sum_{J_i=J_{f1}-1}^{J_i=J_{f1}+1} g(E_i, J_i)}$$

$$f(E_{\gamma 2}) \propto \frac{N_{D2}}{E_{\gamma 2}^3 \sum_{[J_{f2}]} \sum_{J_i=J_{f2}-1}^{J_i=J_{f2}+1} g(E_i, J_i)}. \quad (16)$$

In synergy with the methods introduced above, such a pair of γSF data points is internally normalized and we can determine a γSF data-point pair for each E_i. The double sum can be omitted if the two diagonals include one final level each of the same J^π. However, such diagonals are often difficult to identify in the data, and it is more common to observe different spins for two diagonals, such as the 0^+ ground state and the first-exited 2^+ state in even-even nuclei.

Figure 2 illustrates a sewing technique that allows one to connect pairs of γSF data points and is the final step of the shape method to obtain the functional form of the γSF. In this example, we show three different pairs, each from a different E_i, marked by filled circle, square, and triangle data points. The second and third γSF pairs are scaled as explained in the figure caption. In detail, this is accomplished by finding a matching-point energy, which is chosen to be the average γ-ray energy $E_{\gamma\text{ave}}$ of the two extreme γSF data points of two neighboring pairs. Generally, the deviations between adjacent, matched pairs are larger when using a linear interpolation. Therefore, we use a logarithmic interpolation of the γSF data points for each pair to $E_{\gamma\text{ave}}$. The resulting sewed γSF is represented by the black line to guide the eye in panel (c) and exhibits the shape of the γSF.

IV. SHAPE METHOD ANALYSIS AND RESULTS

In the following, when referring to discrete final levels within the diagonals, we always refer to levels in the data base from the National Nuclear Data Center (NNDC) [51].

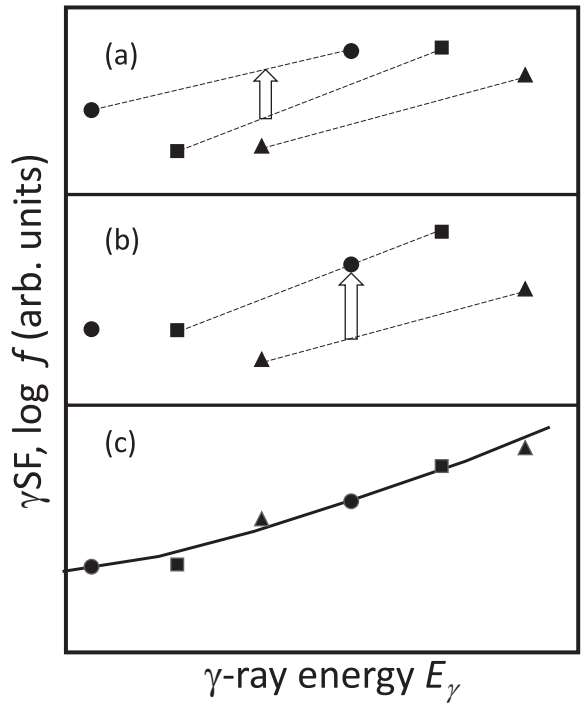

FIG. 2. Illustration of the sewing technique for three γSF pairs (filled circles, squares, and triangles) with each pair connected by dashed lines in (a). The matching-point energy is chosen to be the average (location of arrows) γ-ray energy $E_{\gamma\text{ave}}$ of the two extreme (lowest and highest) γSF data points of two neighboring pairs. The second pair of data points (filled squares) is scaled by a factor to match the first pair of data points at a location indicated by the arrow (filled circles) (a). Then the third pair of data points (filled triangles) is scaled to match the previously corrected data pair (filled squares) at the location of the arrow (b). Finally, the resulting sewed γSF is presented in (c) (solid black line).

For each application of the shape method we use a first-generation matrix with ≈30–40 keV/channel on both axes from which the numbers of counts are determined through integration. These are then further compressed into bins of ≈120 keV/channel unless otherwise noted. The statistical uncertainties are included for each data point through error bars. The observed spread between neighboring matched data points is reflective of the uncertainty band due to the sewing method, e.g., logarithmic interpolation. Detailed discussions on the comparisons of the results from the shape and Oslo methods are deferred to Sec. V.

A. Diagonals with the same final J^π: ^{56}Fe

We utilize data from the ^{56}Fe$(p, p'\gamma)^{56}$Fe reaction previously presented in Refs. [29,30], where the γ rays were measured with six large-volume $LaBr_3$(Ce) detectors from the HECTOR$^+$ array [52] and the charged particles with the SiRi silicon telescope [53]. Figure 3(a) shows the resulting $P(E_\gamma, E_i)$ matrix of ^{56}Fe. Gates were set on the diagonals and correspond to the direct decays to the 2_1^+ (diagonal D_1) and 2_2^+ (diagonal D_2) levels at 847 and 2658 keV in ^{56}Fe, respectively. As the spins and parities for the two final levels are the same,

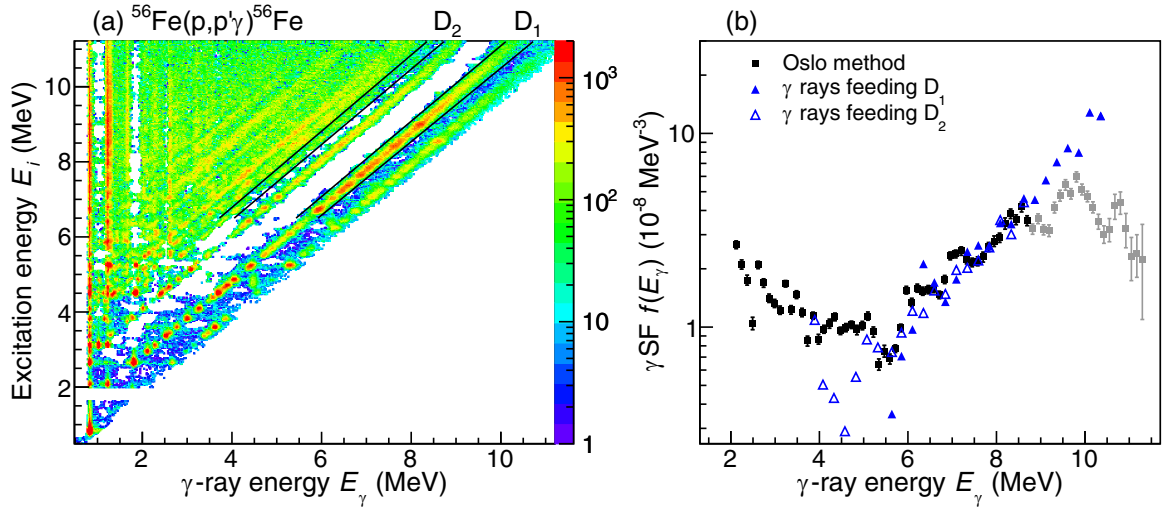

FIG. 3. (a) The first-generation matrix $P(E_\gamma, E_i)$ of ^{56}Fe showing the cuts on the diagonals decaying to the 2_1^+ level (D_1) at $E_f = 847$ keV and the 2_2^+ level (D_2) at $E_f = 2658$ keV. (b) The resulting γSF from the shape method (filled and open blue triangles) compared to the Oslo method results (solid black squares) [29] normalized with the spin-cutoff parameter given by the rigid-body moment of inertia [36]. At the highest γ-ray energies the Oslo method (solid grey squares) is affected by the empty region in the matrix (see text for details). Note that the bin width is 248 keV/channel in this case due to ^{56}Fe being a relatively light nucleus with a low level density. The shape method data points are multiplied by a common absolute-normalization factor, which is found by a χ^2 fit to the Oslo data in the approximate γ-energy region $6 \leqslant E_\gamma \leqslant 8$ MeV.

the initial level density $\rho(E_i)$ and the population-depopulation factor $\sigma(E_i, J_i)g(E_i, J_i)$ of the initial levels that feed the final states in the diagonals are also the same. Therefore, the number of counts in the diagonals for a given E_i only needs to be corrected by the E_γ^3 factor. Following the sewing steps outlined above for the pairs of intensities for each E_i, the shape of the γSF is obtained and compared to the results of the Oslo method in Fig. 3(b). The γSF at the highest γ-ray energies obtained with the Oslo method are affected by the empty region between D_1 and the 4_1^+ diagonal. As these pixels with zero counts are included in the global, simultaneous fit of the NLD and γSF, the NLD is (close to) zero in between the discrete levels, and the γSF is accordingly strongly suppressed as there are no levels for decay to occur.

Due to the lack of neutron-resonance spacing data for ^{56}Fe, as ^{55}Fe is unstable, previous works have relied on systematics from nuclear data to obtain the slope of the NLD and γSF [29,30]. Comparing the previous results with those of the new shape method, we can conclude that the two normalizations previously used [29] are indeed reasonable. However, as there is only a ≈30% relative change in the estimated NLD at S_n, with $\rho(S_n) = 2.18(59) \times 10^3$ MeV^{-1} (based on the phenomenological spin-cutoff parameter of Ref. [54]) and $2.87(68) \times 10^3$ MeV^{-1} (spin-cutoff parameter given by rigid-body moment of inertia from Refs. [36,37]) between the two normalizations, we are not in a position to confirm which normalization is correct. If there was a more pronounced discrepancy in slope between the different normalizations, the present method may enable a discrimination between the input spin-distribution models. We would like to point out that the previous approach of utilizing systematics for the determination of D_0 in ^{56}Fe [29] appears to be appropriate in this case. However, there is no reason to assume that such a methodology based on systematics can be applied in general. Hence, if no reliable systematics can be made, such as for nuclei far away from stability, the present method, which is based on a sound foundation, clearly provides a significant constraint on the slope of the NLD and γSF. The low- and high-energy discrepancies observed in Fig. 3(b) are further explored in Sec. V.

B. Several diagonals with different final J^π combinations: ^{92}Zr

Data from the (p, p') reaction populating ^{92}Zr [31] were used with the γ rays detected in the NaI(Tl) CACTUS array [55] and the charged particles in SiRi. With $N = 52$, ^{92}Zr is close to the magic $N = 50$ shell closure and is characterized by few low-lying levels. With the present experimental resolution it is possible to identify four diagonals. With the six combinations D_1D_2, D_1D_3, D_1D_4, D_2D_3, D_2D_4, and D_3D_4 one can investigate the consistency between the various γSFs from the shape and Oslo method results.

Figure 4(a) shows the primary matrix with the diagonals D_j which include the following discrete states:

D_1: 0^+(0 keV).
D_2: 2^+(934 keV).
D_3: 0^+(1383 keV) and 4^+(1495 keV).
D_4: 3^-(2340 keV), 4^+(2398 keV), and 5^-(2486 keV).

The lower part of the matrix shows that many nonstatistical γ-ray transitions connect discrete levels and it is important to point out that these should not be taken into account when extracting the average γSF for ^{92}Zr. Thus, the results for the Oslo method in Fig. 4(b) were extracted for $E_i > 4.5$ MeV.

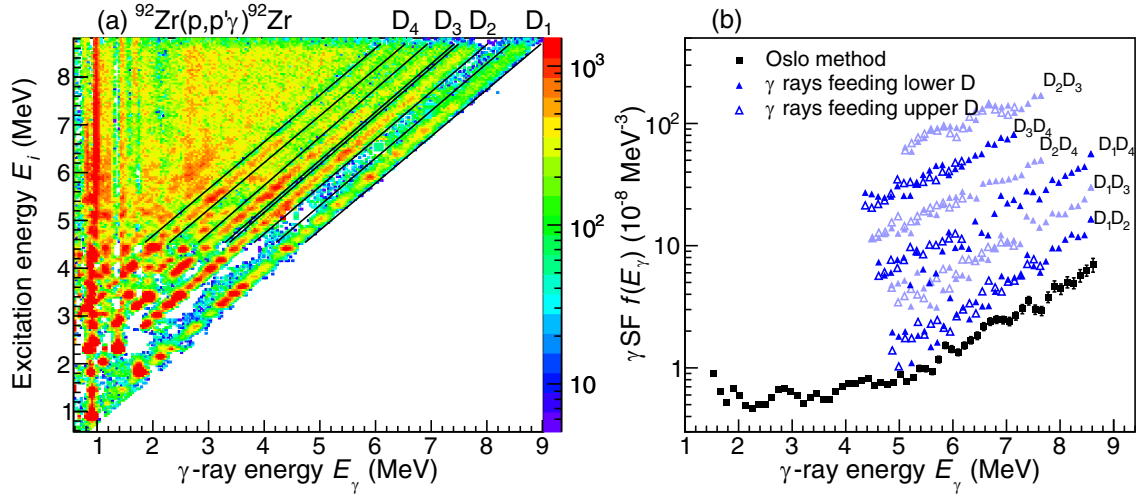

FIG. 4. (a) The first-generation matrix $P(E_\gamma, E_i)$ of ^{92}Zr showing the four diagonals described in the text. (b) The resulting γSFs from the shape method (filled and open triangles in blue and light blue) compared to the Oslo method results (black squares). The individual shape method results are shifted in the plot in order to visualize the results from the various combinations of diagonals. The shape method data points are multiplied by a common absolute-normalization factor, which is found by a χ^2 fit to the Oslo data in the approximate γ-energy region $5 \leqslant E_\gamma \leqslant 7$ MeV.

Similarly, when applying the shape method it is imperative to remain above E_i values with enough initial states within the energy bin at E_i that feed the levels contained by the diagonals. For ^{92}Zr we obtain erratic fluctuations for $E_\gamma < 5$ MeV and these data are not shown.

It is gratifying that the six extracted γSFs from the shape method are all in rather good agreement with the functional form between each other and the one obtained with the Oslo method. Since the combination of diagonals represent a variety of final J^π values, yet they provide consistent functional forms, the spin distribution $g(E, J)$ applied in Eq. (5) with spin cutoff parameters of Table I is supported.

C. Diagonals including ground and two-quasiparticle bands: ^{164}Dy

For rare earth nuclei, the level density becomes high enough that it is difficult to identify final levels in the $P(E_\gamma, E)$ matrix within the experimental resolutions. However, the known levels of ^{164}Dy group into the ground-state band between 0 and 0.5 MeV and two-quasiparticle band structures around 1.1 MeV. Figure 5 illustrates the level density obtained with the Oslo method, and displays these two relatively well-defined structures. This makes ^{164}Dy a feasible case for applying the shape method to the ^{164}Dy(^{3}He, ^{3}He′) experimental data, measured with the CACTUS and SiRi arrays, from Refs. [32,56,57]. Furthermore, there are two interesting features in the previous findings of the γSF: (i) a scissors resonance at $E_\gamma = 2.83(8)$ MeV is built on the tail of the giant dipole resonance and (ii) it has been speculated that an enhancement exists around $E_\gamma = 6$–7 MeV due to the $E1$ pygmy resonance [32]. From the matrix in Fig. 6(a) we recognize the diagonals corresponding to the ground-state and two-quasiparticle bands. Here, diagonal D_1 includes the 0^+, 2^+, 4^+, and 6^+ levels of the ground state band in the excitation region of 0–0.5 MeV. Diagonal D_2 includes 14 levels in the excitation region of 0.76–1.39 MeV, all with known J^π [51]. Figure 6(b) shows the γSF extracted with the Oslo method [32] together with the shape method results. The highest γ-ray energies above ≈7 MeV are located in a region that is possibly affected by structural effects. Here, the decay goes to the ground-state band, for which the NLD is overestimated, as is apparent from Fig. 5. This could be due to a strong overlap and thus dependence of the initial levels and the ground band, with the possible consequence of the NLD and γSF not being

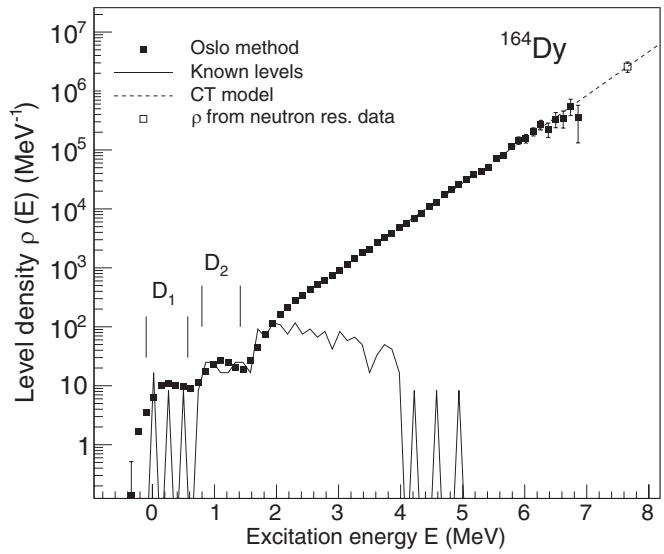

FIG. 5. Level densities of ^{164}Dy [57]. The solid line represents the NLD of known levels. The filled square symbols show the results of the Oslo method. The data points are connected to the NLD at S_n (open square) through extrapolation with the constant temperature (CT) model.

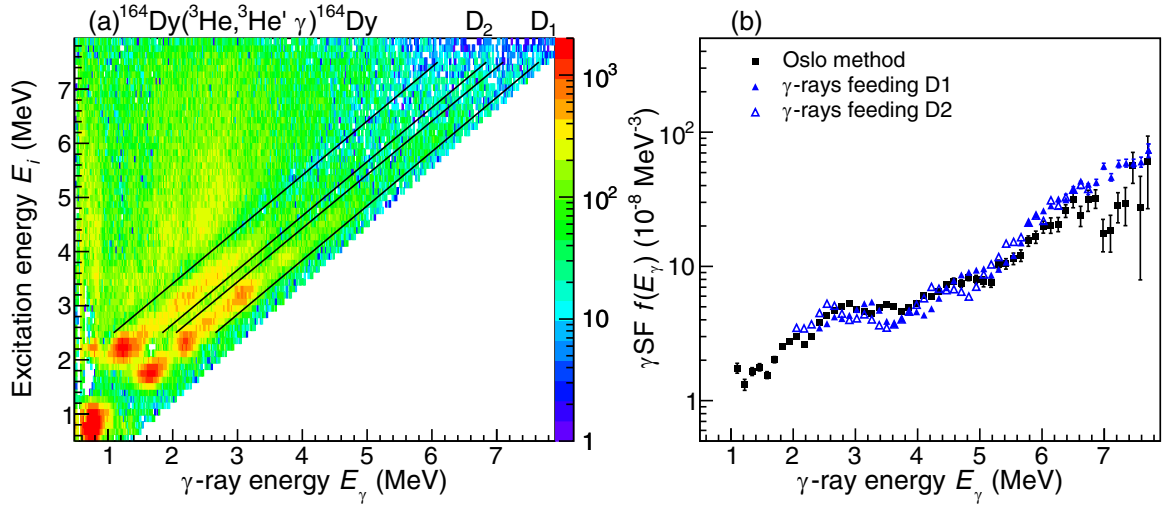

FIG. 6. (a) The first-generation matrix $P(E_\gamma, E_i)$ of ^{164}Dy showing the two diagonals described in the text. (b) The resulting γSF from the shape method (filled and open blue triangles) compared to the Oslo method results (black squares). The shape method data points are multiplied by a common absolute-normalization factor, which is found by a χ^2 fit to the Oslo data in the approximate γ-energy region $2 \leqslant E_\gamma \leqslant 6.5$ MeV.

fully decoupled. Thus, an overestimate of the NLD at low E_x could lead to a suppressed γSF at the highest E_γ values.

As the D_0 value is in fact known for ^{164}Dy, the overall very good agreement with the slope of the γSF from the regular Oslo normalization provides support for the applicability of the shape method. It is interesting to note that the scissors resonance is directly visible from Fig. 6(a) as a yellow-shaded region for $E_i > 4$ MeV and $E_\gamma \approx 2$–3 MeV. This enhanced intensity is the main contributor to the scissors resonance strength obtained with the Oslo method. It is therefore rather exciting that the same information is also contained in the two diagonals used in the shape method, resulting in a similar enhancement for $E_\gamma \approx 2$–3 MeV.

Furthermore, the shape method provides data up to S_n with an apparent deviation in slope at $E_\gamma \approx 5.5$ MeV, which may signal the presence of a resonance located in the $E_\gamma \approx 6$–7 MeV region. The previous results using the Oslo method were hampered by a reduced γSF at the highest energies, due to structural effects at low energies, as indicated by the data points in Fig. 6(b) for $E_\gamma > 6.6$ MeV, and therefore did not allow for a strong statement regarding the existence of an enhancement [32].

V. DISCUSSION

The shapes of the γSFs extracted with the Oslo method are reasonably well reproduced with the shape method, in particular for excitation energies for which the total NLD of initial states is high. With reduced excitation energies discrete structures may become dominant and the concepts of γSF and NLD are no longer applicable. This situation is apparent when inspecting the γSF of ^{56}Fe in Fig. 3(b) where the γSF below $E_\gamma \approx 5.5$ MeV ($E_i \approx 6.5$ MeV) exhibits significant fluctuations. The NLD at $E_i = 6$ MeV has been measured to be $\rho \approx 100$ MeV^{-1} [58]. For ^{92}Zr the shape method has been applied from $E_i = 4.5$ MeV where $\rho \approx 180$ MeV^{-1} [31]. For the heavier nucleus ^{164}Dy the level density reaches $\rho \approx 800$ MeV^{-1} at $E_i = 3$ MeV, as is evident from Fig. 5. The relatively high NLD found in ^{164}Dy allows for the shape method to be applied to low enough E_i values to cover the range of the scissors resonance. It is important to emphasize that careful considerations have to be given to identify appropriate E_i regions for the shape method to be applicable. Discrete states and/or structures may become dominant features which lie outside the statistical regime. This is particularly the case for light A nuclei or those which are located near closed shells. From our investigation, a minimum of $\rho \approx 100$ MeV^{-1} appears to be appropriate, or, more specifically, one should have more than $\approx$10 transitions from excitation energies where compound decay dominates, connecting the initial and final excitation energy bins to reduce the effect of Porter-Thomas fluctuations [59]. These values are estimates and it is strongly recommended that each nucleus be investigated carefully to determine the lowest reliable E_i and hence lowest γ-ray energy to be used.

At higher E_i, the data points from the shape method follow the functional form of the γSFs from the Oslo method rather well. At the highest E_i, the Oslo method may underestimate the γSF due to structural effects, whereas the shape method remains robust in this regime. As demonstrated for the three nuclei under consideration, it is in the region of higher γ-ray energies where the slope of the γSF can be reliably obtained with the shape method and provides the necessary constraints if alternative normalization procedures are not possible due to the absence of neutron resonance data.

Nuclei such as ^{56}Fe, for which two low-lying discrete states of the same J^π can be separated experimentally, represent the most fundamental application of the shape method and can be treated with the fewest assumptions and without any model input. In such cases, the NLD and cross section dependencies of primary transitions feeding the states are eliminated.

The shape method remains applicable even when the discrete levels differ in J^π or if the states cannot be resolved experimentally. This is clearly demonstrated for ^{92}Zr, where

six different combinations of final levels all yield strikingly similar functional forms of the γSF. This illustrates the robustness of the applied spin distributions and the assumption that the population cross section is proportional to the spin distribution over the E_i ranges considered for the extraction of γSF below the particle thresholds.

The results from ^{164}Dy further reveal that the inclusion of many final levels of widely varying J^π values or even distinctive nuclear structures still leads to an energy dependence which is similar to that of the γSFs from the Oslo method. The ^{164}Dy Oslo method results show the presence of the scissors resonance. The same information is retained in both diagonals and the resonance is observed by the shape method. This may imply that this resonance is a collective mode obeying the Brink-Axel hypothesis [60–63]. A suspected pygmy resonance at $E_\gamma \approx 6$–7 MeV is apparent through the changing slope in ^{164}Dy, while previous results were inconclusive [32], highlighting the complementary nature of the shape method.

It is interesting to note that the results from the shape method clearly yield very similar γSFs, regardless if the γSFs are built on different nuclear structures or J^π states of a given nucleus. This confirms the validity of the generalized Brink-Axel hypothesis, supporting previous results [26–29]. Another appealing aspect of the shape method is the fact that it can be applied to the same set of experimental data as that used to extract the NLD and γSF with the Oslo method. This is highly beneficial when the shape method is used to specifically determine the slope for the NLD and γSF from the Oslo method since it avoids unnecessary additional systematic uncertainties which would arise when performing different experiments.

VI. SUMMARY

It has long been a challenging endeavor to estimate the slope of the γSF in the absence of neutron resonance data, which is compounded by the fact that no standardized approach exists which is applicable to all nuclei. The shape method provides a solution to the γSF normalization conundrum when D_0 values are not available. It provides a standardized approach to determine the slope of the γSF and NLD (if extracted simultaneously through the Oslo method), which is not only universally applicable but will also provide consistency for analyses and results.

The shape method makes use of concepts from the average resonance capture, ratio, and χ^2 methods and is based on the unambiguous experimental identification of the origin and destination of primary γ-ray transitions. Through their intensities, pairs of primary transitions retain the information on the functional form of the γSF.

The shape method has been applied to three nuclei which are representative of the typical situations encountered: (i) low-mass ^{56}Fe, (ii) ^{92}Zr located in the vicinity of shell closures, and (iii) ^{164}Dy with scissors and pygmy resonances. These three nuclei further represent a variety of J^π combinations for low-lying states which are fed by the primary transitions. In ^{56}Fe, the primary transitions feed two well-separated and experimentally resolved states of the same J^π, while in ^{92}Zr some of the low-lying states cannot be resolved and are of different J^π. For ^{164}Dy the low-lying states can only be identified through clusters of specific nuclear structures in the form of the ground and two-quasiparticle bands. Regardless of the intricacies and details of the individual nuclei considered, the shape method extracts functional forms of γSFs which are consistent with those from the Oslo method. This highlights the robustness of the method and, where applicable, the appropriateness of the assumptions made regarding the spin distributions. While the shape method provides a universal prescription to determine the slope of the γSF (and for the NLD in the case of the Oslo method) in the absence of experimentally measured neutron resonance spacing it does not provide the absolute values of the γSFs when neutron resonance widths are not available. Further work is highly desirable to explore alternate approaches to determine the absolute values of γSFs.

Complementary to this work, we have also applied the shape method to ^{76}Ge and ^{88}Kr for the extraction of model-independent nuclear level densities away from stability [21].

ACKNOWLEDGMENTS

This work is based on research supported in part by the National Research Foundation of South Africa (Grant No. 118846), by the Research Council of Norway (Grant No. 263030), the National Science Foundation (Grant No. PHY 1913554), the DOE National Nuclear Security Administration through Grant No. DOE-DE-NA0003906, the Nuclear Science and Security Consortium, under Award No. DE-NA0003180, and by the Department of Energy, Office of Nuclear Physics, under Grant No. DE-SC0020451. A.C.L. acknowledges funding of this research by the European Research Council through ERC-STG-2014 under Grant Agreement No. 637686, support from the "ChETEC" COST Action (CA16117), COST (European Cooperation in Science and Technology), and from JINA-CEE through the National Science Foundation under Grant No. PHY-1430152 (JINA Center for the Evolution of the Elements).

[1] S. Goriely, P. Dimitriou, M. Wiedeking, T. Belgya, R. Firestone, J. Kopecky *et al.*, Eur. Phys. J. A **55**, 172 (2019).
[2] M. Arnould, S. Goriely, and K. Takahashi, Phys. Rep. **450**, 97 (2007).
[3] M. Mumpower, R. Surman, G. McLaughlin, and A. Aprahamian, Prog. Part. Nucl. Phys. **86**, 86 (2016).
[4] A. C. Larsen, A. Spyrou, S. N. Liddick, and M. Guttormsen, Prog. Part. Nucl. Phys. **107**, 69 (2019).
[5] M. Arnould and S. Goriely, Prog. Part. Nucl. Phys. **112**, 103766 (2020).
[6] B. V. Kheswa, M. Wiedeking, F. Giacoppo, S. Goriely, M. Guttormsen, A. C. Larsen *et al.*, Phys. Lett. B **744**, 268 (2015).

[7] A. Spyrou, S. N. Liddick, A. C. Larsen, M. Guttormsen, K. Cooper, A. C. Dombos *et al.*, Phys. Rev. Lett. **113**, 232502 (2014).

[8] A. C. Larsen, M. Guttormsen, R. Schwengner, D. L. Bleuel, S. Goriely, S. Harissopulos *et al.*, Phys. Rev. C **93**, 045810 (2016).

[9] K. L. Malatji, M. Wiedeking, S. Goriely, C. P. Brits, B. V. Kheswa, F. L. B. Garrote *et al.*, Phys. Lett. B **791**, 403 (2019).

[10] W. Hauser and H. Feshbach, Phys. Rev. **87**, 366 (1952).

[11] A. Schiller, L. Bergholt, M. Guttormsen, E. Melby, J. Rekstad, and S. Siem, Nucl. Instrum. Methods A **447**, 498 (2000).

[12] M. Wiedeking, L. A. Bernstein, M. Krtička, D. L. Bleuel, J. M. Allmond, M. S. Basunia *et al.*, Phys. Rev. Lett. **108**, 162503 (2012).

[13] M. Krtička, M. Wiedeking, F. Bečvař, and S. Valenta, Phys. Rev. C **93**, 054311 (2016).

[14] M. D. Jones, A. O. Macchiavelli, M. Wiedeking, L. A. Bernstein, H. L. Crawford, C. M. Campbell *et al.*, Phys. Rev. C **97**, 024327 (2018).

[15] S. N. Liddick, A. Spyrou, B. P. Crider, F. Naqvi, A. C. Larsen, M. Guttormsen *et al.*, Phys. Rev. Lett. **116**, 242502 (2016).

[16] B. V. Kheswa, M. Wiedeking, J. A. Brown, A. C. Larsen, S. Goriely, M. Guttormsen *et al.*, Phys. Rev. C **95**, 045805 (2017).

[17] C. P. Brits, K. L. Malatji, M. Wiedeking, B. V. Kheswa, S. Goriely, F. L. Garrote *et al.*, Phys. Rev. C **99**, 054330 (2019).

[18] A. C. Larsen, M. Guttormsen, M. Krtička, E. Běták, A. Bürger, A. Görgen *et al.*, Phys. Rev. C **83**, 034315 (2011).

[19] S. N. Liddick, A. C. Larsen, M. Guttormsen, A. Spyrou, B. P. Crider, F. Naqvi *et al.*, Phys. Rev. C **100**, 024624 (2019).

[20] V. W. Ingeberg, S. Siem, M. Wiedeking, K. Sieja, D. L. Bleuel, C. P. Brits *et al.*, Eur. Phys. J. A **56**, 68 (2020).

[21] D. Mücher, A. Spyrou, H. Berg, M. Wiedeking, M. Guttormsen, A. C. Larsen *et al.*, arXiv:2011.01071.

[22] M. Guttormsen, T. S. Tveter, L. Bergholt, F. Ingebretsen, and J. Rekstad, Nucl. Instrum. Methods A **374**, 371 (1996).

[23] M. Guttormsen, T. Ramsøy, and J. Rekstad, Nucl. Instrum. Methods A **255**, 518 (1987).

[24] J. E. Midtbø, F. Zeiser, E. Lima, A.-C. Larsen, G. M. Tveten, M. Guttormsen, F. L. B. Garrote, A. Kvellestad, and T. Renstrøm, Comput. Phys. Commun. **262**, 107795 (2021).

[25] D. M. Brink, Nucl. Phys. **4**, 215 (1957).

[26] M. Guttormsen, A. C. Larsen, A. Görgen, T. Renstrøm, S. Siem, T. G. Tornyi, and G. M. Tveten, Phys. Rev. Lett. **116**, 012502 (2016).

[27] M. Markova, P. von Neumann-Cosel, A. C. Larsen, S. Bassauer, A. Görgen, M. Guttormsen *et al.*, arXiv:2012.11956.

[28] L. C. Campo, M. Guttormsen, F. L. Bello Garrote, T. K. Eriksen, F. Giacoppo, A. Görgen *et al.*, Phys. Rev. C **98**, 054303 (2018).

[29] A. C. Larsen, M. Guttormsen, N. Blasi, A. Bracco, F. Camera, L. C. Campo *et al.*, J. Phys. G: Nucl. Part. Phys **44**, 064005 (2017).

[30] A. C. Larsen, N. Blasi, A. Bracco, F. Camera, T. K. Eriksen, A. Görgen *et al.*, Phys. Rev. Lett. **111**, 242504 (2013).

[31] M. Guttormsen, S. Goriely, A. C. Larsen, A. Görgen, T. W. Hagen, T. Renstrøm *et al.*, Phys. Rev. C **96**, 024313 (2017).

[32] T. Renstrøm, H. Utsunomiya, H. T. Nyhus, A. C. Larsen, M. Guttormsen, G. M. Tveten *et al.*, Phys. Rev. C **98**, 054310 (2018).

[33] T. Ericson, Adv. Phys. **9**, 425 (1960).

[34] A. J. Koning, S. Hilaire, and S. Goriely, Nucl. Phys. A **810**, 13 (2008).

[35] R. Capote, M. Herman, P. Obložinský, P. G. Young, S. Goriely, T. Belgya *et al.*, Nucl. Data Sheets **110**, 3107 (2009).

[36] T. von Egidy and D. Bucurescu, Phys. Rev. C **72**, 044311 (2005).

[37] T. von Egidy and D. Bucurescu, Phys. Rev. C **73**, 049901(E) (2006).

[38] S. Mughabghab, *Atlas of Neutron Resonances: Resonance Parameters and Thermal Cross Sections* $Z = 1$*–100*, 5th ed. (Elsevier, Amsterdam, 2006).

[39] A. Gilbert and A. G. W. Cameron, Can. J. Phys. **43**, 1446 (1965).

[40] T. Ericson, Nucl. Phys. **11**, 481 (1959).

[41] S. Goriely, S. Hilaire, and A. J. Koning, Phys. Rev. C **78**, 064307 (2008).

[42] J. Kopecky and M. Uhl, Phys. Rev. C **41**, 1941 (1990).

[43] M. Guttormsen, F. Zeiser, J. E. Midtbø, V. W. Ingeberg, and A. C. Larsen, Oslo method software v1.1.4, 2020.

[44] L. M. Bollinger and G. E. Thomas, Phys. Rev. C **2**, 1951 (1970).

[45] R. Chrien, J. Kopecky, H. Liou, O. Wasson, J. Garg, and M. Dritsa, Nucl. Phys. A **436**, 205 (1985).

[46] J. Kopecky, S. Goriely, S. Péru, S. Hilaire, and M. Martini, Phys. Rev. C **95**, 054317 (2017).

[47] Z. Szeflínski and G. Szeflínska, Z. Wilhelmi, T. Rzaca-Urban, H. Klapdor, E. Anderson, K. Grotz, and J. Metzinger, Nucl. Phys. A **323**, 253 (1979).

[48] B. Erlandsson, K. Nilson, and A. Marcinkowski, Nucl. Phys. A **329**, 1 (1979).

[49] J. Isaak, D. Savran, B. Löher, T. Beck, M. Bhike, U. Gayer *et al.*, Phys. Lett. B **788**, 225 (2019).

[50] P. Scholz, M. Guttormsen, F. Heim, A. C. Larsen, J. Mayer, D. Savran *et al.*, Phys. Rev. C **101**, 045806 (2020).

[51] Data extracted from NuDat database of the National Nuclear Data Center, Brookhaven National Laboratory, USA, as of September 2018.

[52] A. Giaz, L. Pellegri, S. Riboldi, F. Camera, N. Blasi, C. Boiano *et al.*, Nucl. Instrum. Methods A **729**, 910 (2013).

[53] M. Guttormsen, A. Bürger, T. E. Hansen, and N. Lietaer, Nucl. Instrum. Methods A **648**, 168 (2011).

[54] T. von Egidy and D. Bucurescu, Phys. Rev. C **80**, 054310 (2009).

[55] M. Guttormsen A. Atac, G. Løvhøiden, S. Messelt, T. Ramsøy, J. Rekstad, T. F. Thorsteinsen, T. S. Tveter, and Z. Zelazny, Phys. Scr. **1990**, 54 (1990).

[56] H. T. Nyhus, S. Siem, M. Guttormsen, A. C. Larsen, A. Bürger, N. U. H. Syed, G. M. Tveten, and A. Voinov, Phys. Rev. C **81**, 024325 (2010).

[57] H. T. Nyhus, S. Siem, M. Guttormsen, A. C. Larsen, A. Bürger, N. U. H. Syed, H. K. Toft, G. M. Tveten, and A. Voinov, Phys. Rev. C **85**, 014323 (2012).

[58] E. Algin, U. Agvaanluvsan, M. Guttormsen, A. C. Larsen, G. E. Mitchell, J. Rekstad, A. Schiller, S. Siem, and A. Voinov, Phys. Rev. C **78**, 054321 (2008).

[59] C. E. Porter and R. G. Thomas, Phys. Rev. **104**, 483 (1956).

[60] M. Krtička, F. Bečvář, J. Honzátko, I. Tomandl, M. Heil, F. Käppeler, R. Reifarth, F. Voss, and K. Wisshak, Phys. Rev. Lett. **92**, 172501 (2004).

[61] M. Guttormsen, L. A. Bernstein, A. Bürger, A. Görgen, F. Gunsing, T. W. Hagen *et al.*, Phys. Rev. Lett. **109**, 162503 (2012).

[62] J. Kroll, B. Baramsai, G. E. Mitchell, U. Agvaanluvsan, F. Bečvář, T. A. Bredeweg *et al.*, Phys. Rev. C **88**, 034317 (2013).

[63] M. Guttormsen, L. A. Bernstein, A. Görgen, B. Jurado, S. Siem, M. Aiche *et al.*, Phys. Rev. C **89**, 014302 (2014).